# Mechanism of spike frequency adaptation in substantia gelatinosa neurones of rat

Igor V. Melnick[1], Sónia F. A. Santos[1,2] and Boris V. Safronov[1,2]

[1] *Instituto de Biologia Molecular e Celular, Rua do Campo Alegre 823, 4150-180 Porto, Portugal and* [2] *Instituto de Histologia e Embriologia, Faculdade de Medicina, Universidade do Porto, Alameda Professor Hernâni Monteiro, 4200-319 Porto, Portugal*

**Using tight-seal recordings from rat spinal cord slices, intracellular labelling and computer simulation, we analysed the mechanisms of spike frequency adaptation in substantia gelatinosa (SG) neurones. Adapting-firing neurones (AFNs) generated short bursts of spikes during sustained depolarization and were mostly found in lateral SG. The firing pattern and the shape of single spikes did not change after substitution of $Ca^{2+}$ with $Co^{2+}$, $Mg^{2+}$ or $Cd^{2+}$ indicating that $Ca^{2+}$-dependent conductances do not contribute to adapting firing. Transient $K_A$ current was small and completely inactivated at resting potential suggesting that adapting firing was mainly generated by voltage-gated $Na^+$ and delayed-rectifier $K^+$ ($K_{DR}$) currents. Although these currents were similar to those previously described in tonic-firing neurones (TFNs), we found that $Na^+$ and $K_{DR}$ currents were smaller in AFNs. Discharge pattern in TFNs could be reversibly converted into that typical of AFNs in the presence of tetrodotoxin but not tetraethylammonium, suggesting that lower $Na^+$ conductance is more critical for the appearance of firing adaptation. Intracellularly labelled AFNs showed specific morphological features and preserved long extensively branching axons, indicating that smaller $Na^+$ conductance could not result from the axon cut. Computer simulation has further revealed that down-regulation of $Na^+$ conductance represents an effective mechanism for the induction of firing adaptation. It is suggested that the cell-specific regulation of $Na^+$ channel expression can be an important factor underlying the diversity of firing patterns in SG neurones.**

(Resubmitted 13 April 2004; accepted after revision 25 June 2004; first published online 2 July 2004)
**Corresponding author** Boris V. Safronov: Instituto de Biologia Molecular e Celular, Rua do Campo Alegre 823, 4150-180 Porto, Portugal. Email: safronov@ibmc.up.pt

The dorsal horn of the spinal cord is the first relay station processing the sensory input from primary afferent terminals. The diversity of sensory modalities in dorsal horn is encoded by the type of peripheral afferent fibre, synaptic connectivity and intrinsic firing properties of dorsal horn neurones (Brown, 1981; Cervero, 1987; Willis & Coggeshall, 1991). The substantia gelatinosa (SG) is the dorsal horn region where most fine-calibre C- and A$\delta$-fibres terminate (Rethelyi, 1977; LaMotte, 1977; Light & Perl, 1977; Sugiura *et al.* 1986) and is therefore considered to be a key element in the nociceptive processing system.

Several classes of SG neurones are distinguished on the basis of their intrinsic firing properties (Yoshimura & Jessell, 1989; Thomson *et al.* 1989; Lopez-Garcia & King, 1994; Grudt & Perl, 2002). A major criterion widely used for such a classification is a degree of spike frequency adaptation observed during sustained membrane depolarization. While some neurones were characterized by a tonic firing, the others exhibited a strong adaptation generating short bursts of spikes or just a single spike. A degree of spike frequency adaptation in a neurone correlates with a type of its cutaneous afferent input (Lopez-Garcia & King, 1994) and therefore the cell-specific regulation of firing adaptation can underlie diverse modalities of sensory encoding in SG. In spite of its importance, the mechanism of spike frequency adaptation in SG neurones is not well understood.

Recently we described the ion basis of tonic (non-adapting) firing in a group of SG neurones and created a computer model of the SG neurone (Melnick *et al.* 2004). The voltage-gated $Na^+$ and delayed-rectifier $K^+$ channels were shown to generate the basic pattern of tonic firing, while the $Ca^{2+}$-dependent conductances stabilized firing and regulated discharge frequency. The present study was carried out to elucidate the major

I. V. Melnick and S. F. A. Santos contributed equally to this work.

 DOI: 10.1113/jphysiol.2004.066415

factors responsible for the appearance of spike frequency adaptation in SG neurones.

## Methods

Tight-seal recordings were performed using both 200 $\mu$m transverse and 300 $\mu$m parasagittal slices prepared from the lumbar enlargement of the spinal cord of 2- to 7-week-old rats (Edwards *et al.* 1989; Bentley & Gent, 1994; Chery & De Konink, 2000). The animals were killed in accordance with national guidelines (Direcção Geral de Veterinária, Ministério da Agricultura). After anaesthesia by intraperitoneal injection of sodium pentobarbital (30 mg kg$^{-1}$) the vertebral column was quickly cut out and immersed in ice-cold oxygenated artificial cerebrospinal fluid (ACSF). The 5–7 mm segment of the lumbar enlargement was dissected and the slices were prepared using a tissue slicer (Leica VT 1000S). The slices were then incubated for 30–60 min in ACSF at 33°C. SG (lamina II) was identified as a translucent band in the dorsal horn (Fig. 2*A*). Neurones were localized during recording according to a position of the pipette tip on the video-image of SG.

ACSF contained (mM): NaCl 115, KCl 5.6, $CaCl_2$ 2, $MgCl_2$ 1, glucose 11, $NaH_2PO_4$ 1, $NaHCO_3$ 25 (pH 7.4 when bubbled with a 95% $O_2$–5% $CO_2$). To block $Ca^{2+}$-dependent conductances $Co^{2+}$ (2 mM), $Cd^{2+}$ (0.1 mM) and $Mg^{2+}$ (5 mM) were used. $Co^{2+}$ was equimolarly substituted for $Ca^{2+}$. In experiments with $Cd^{2+}$, $Ca^{2+}$ was omitted and $[Mg^{2+}]$ was increased to 3 mM. In 5 mM $Mg^{2+}$ solution the concentration of $Ca^{2+}$ was reduced to 0.1 mM. The last solution was also used for studying $Na^+$ and $K^+$ channels and is referred to as ACSF*. Standard pipette solution contained (mM): NaCl 15, KCl 120, $MgCl_2$ 1, EGTA 10 and Hepes 10 (pH 7.3 adjusted with KOH, final $[K^+]$ was 151 mM). The solution with low $Ca^{2+}$ buffering capacity contained (mM): NaCl 5, KCl 147, $MgCl_2$ 1, EGTA 1 and Hepes 10 (pH 7.3, adjusted with KOH, final $[K^+]$ was 155 mM). The pipette solution for studying $Na^+$ channels contained (mM): NaCl 4, CsCl 131, $MgCl_2$ 2, EGTA 10 and Hepes 10 (pH 7.3 adjusted by CsOH and NaOH, final $[Cs^+] = 153$ mM and $[Na^+] = 6$ mM). All chemicals were purchased from Sigma.

The patch pipettes were pulled from thick-walled borosilicate glass tubes (Modulohm, Denmark) and had after fire-polishing a resistance of 3–5 MΩ. The EPC-9 amplifier (HEKA, Lambrecht, Germany) was used in all experiments. The effective corner frequency of the low-pass filter was 3 kHz. The frequency of digitization was 10 kHz. Transients and leakage currents were digitally subtracted using standard $P/n$ protocol. Offset potentials were nulled directly before formation of a seal. Liquid junction potentials were calculated and corrected for in all experiments. In neurones subjected to detailed analysis the series resistance measured in the whole-cell mode was 6–20 MΩ and was compensated by at least 60%. Input resistance was measured in both current- and voltage-clamp modes. Ion channels were studied in nucleated patches excised from somatic membrane (Sather *et al.* 1992). To calculate the density of somatic channels, the diameter of each patch was measured.

Action potentials were recorded using the fast current-clamp mode of the EPC-9 amplifier. The accuracy of the voltage measurements done with this patch-clamp amplifier was tested in the experiments shown in Fig. 1. A current pulse (2 nA, 3 ms) was applied to a model circuit containing a capacitor ($C_m$, 22 pF) and a resistor ($R_m$, 500 MΩ) connected in series with another resistor ($R_S$, 5.1 MΩ). A theoretically calculated response (continuous line) was compared with the averaged trace of 500 recordings (dashed line). Time derivatives of both theoretical and recorded voltage traces ($dV/dt$) are shown on the right. In the initial phase of depolarization, the fast current-clamp mode of the EPC-9 amplifier produced less distortion of the recorded signal than the normal (slow) current-clamp mode of the EPC-7 amplifier (see Fig. 3*C* from Magistretti *et al.* 1996, 1998) and it appears to be more suitable for measurements of voltage changes and polarization velocities.

The current–voltage ($I$–$V$) relationship for $Na^+$ channels was fitted using the equation: $G_0/(1 + \exp((V_{50} - V)/k))(V - V_{rev})$, where $G_0$ is the maximum conductance, $V_{50}$ is the potential of

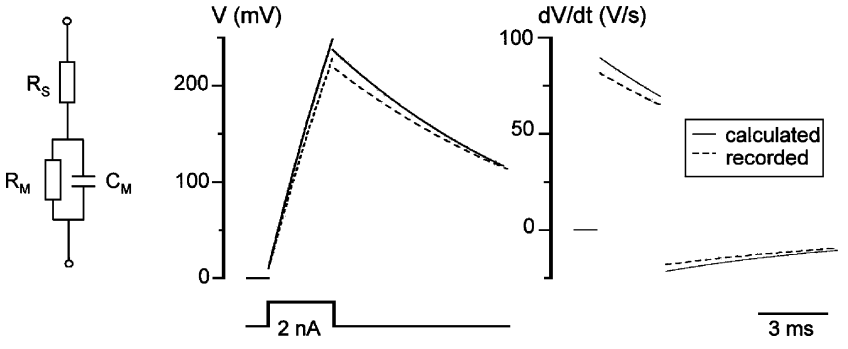


**Figure 1. Test of the voltage change measurements made using the fast current-clamp mode of the EPC-9 amplifier**
Parameters of the model circuit: $C_m = 22$ pF, $R_m = 500$ MΩ and $R_S = 5.1$ MΩ. Current pulse: 2 nA, 3 ms. Continuous line, a theoretically calculated response; dashed line, an average of 500 recorded traces. Right, time derivatives of calculated and recorded voltage traces ($dV/dt$). Points corresponding to instantaneous voltage changes on $R_S$ at the beginning and end of the pulse are removed from both $dV/dt$ graphs.

half-maximum channel activation, $k$ is a steepness factor and $V_{rev}$ is the reversal potential obtained by fitting for each $I$–$V$ curve. $K^+$ conductances were calculated assuming $V_{rev} = E_K = -84$ mV, where $E_K$ is the equilibrium potential for $K^+$. The activation and steady-state inactivation characteristics were fitted with a Boltzmann function: $1/(1 + \exp((V_{50} - V)/k))$. The time course of $Na^+$ channel recovery from inactivation was fitted using a two-exponential function: $1 - A \exp(-t/\tau_F) - (1 - A) \exp(-t/\tau_S)$, where $\tau_F$ and $\tau_S$ are the fast and slow time constants, $A$ is the relative amplitude of the fast component.

All numbers are given as mean ± standard error of the mean (S.E.M.). The values obtained by data fitting with a linear or non-linear least-squares procedures are given as mean ± standard error (S.E.M.). In all figures the error bars

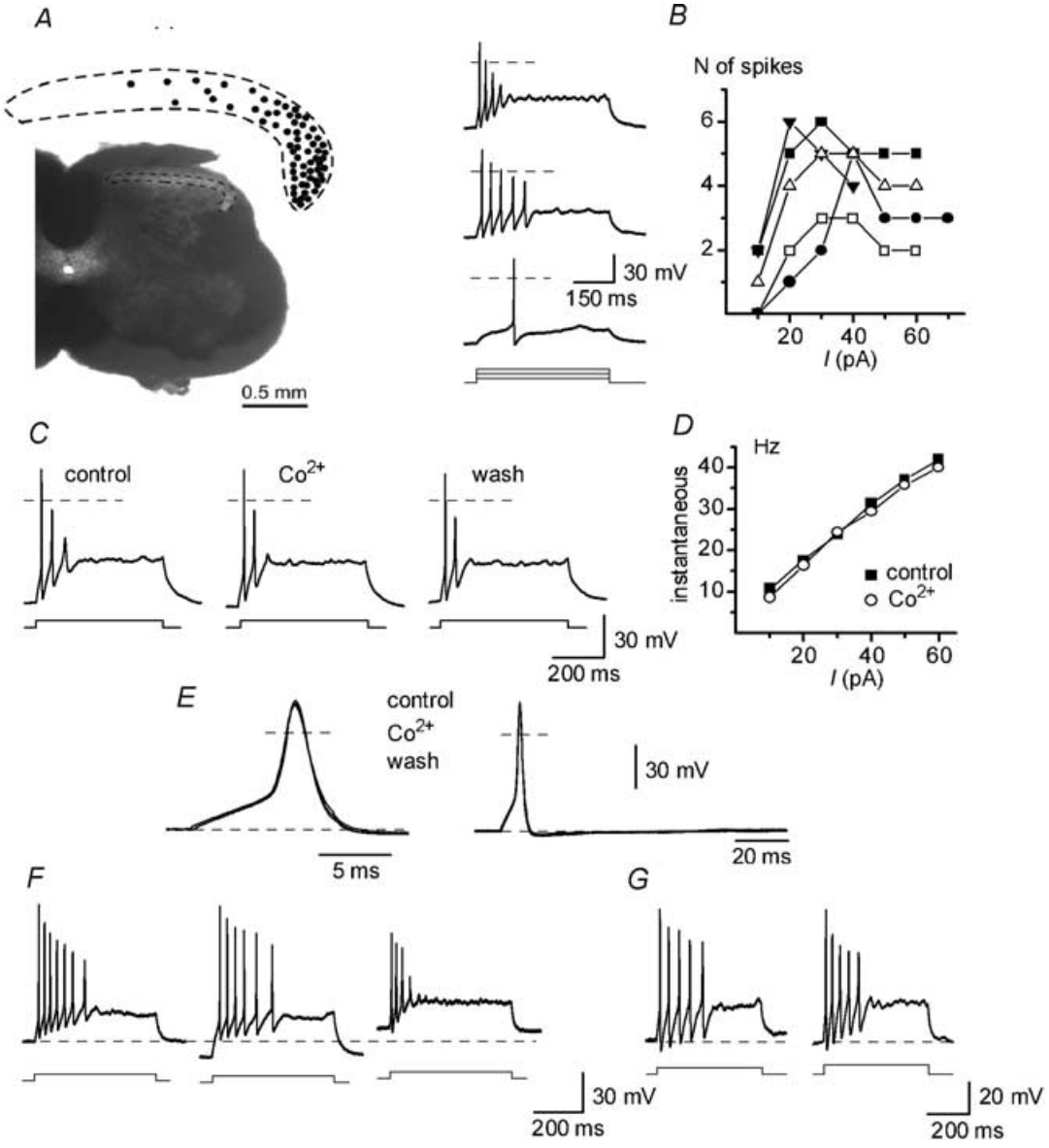


**Figure 2. Discharge properties of adapting-firing neurones (AFNs) in ACSF (2 mM $Ca^{2+}$) and $Ca^{2+}$-free solutions**

*A*, localization of AFNs ($n = 65$) in SG. Transverse section of the spinal cord of 19-day-old rat. *B*, bursts of spikes evoked in an AFN by 0.5 s depolarizing current pulses of 10, 30 and 50 pA in ACSF. Dashed lines, 0 mV. Right, the number of spikes as a function of injected current plotted for 5 AFNs. *C*, firing patterns in ACSF (control and wash) and $Co^{2+}$-containing solution. The stimulation strength was 20 pA in all recordings. *D*, instantaneous frequency–current (*f–I*) characteristics of AFNs in ACSF and $Co^{2+}$-containing solution. *E*, single spikes activated by 10 ms current pulses in ACSF and $Co^{2+}$-containing solution. *F*, discharge patterns in an AFN at varying membrane potentials, −70 mV (dashed line), −80 and −60 mV. *G*, firing patterns recorded in ACSF with external 2.5 mM $K^+$ at room temperature (left) and 35–37°C (right). Current pulses: 20 and 30 pA, respectively.

**Table 1. Comparison of single spike parameters in control and 2 mM $Co^{2+}$**

| Spike parameters | Units | Control | $Co^{2+}$ | Wash | *t* test |
|---|---|---|---|---|---|
| Width at 0 mV | ms | $1.2 \pm 0.1$ | $1.2 \pm 0.1$ | $1.1 \pm 0.1$ | n.s. |
| Width at −30 mV | ms | $2.3 \pm 0.2$ | $2.4 \pm 0.2$ | $2.5 \pm 0.2$ | n.s. |
| Amplitude[a] | mV | $95.2 \pm 3.0$ | $90.5 \pm 2.9$ | $86.3 \pm 2.7$ | n.s. |
| AHP, maximum[b] | mV | $68.1 \pm 1.2$ | $69.2 \pm 1.1$ | $69.6 \pm 1.1$ | n.s. |
| AHP, at 40 ms[c] | mV | $67.1 \pm 1.0$ | $67.8 \pm 0.7$ | $68.6 \pm 0.9$ | n.s. |

[a]The spike amplitude was measured from a membrane potential of −70 mV. [b]The largest after-hyperpolarization (AHP, maximum) was measured within the first 8–15 ms after beginning of the spike. [c]The second measurement of AHP was 40 ms after the beginning of the spike. Data from 10 neurones. Student's paired *t* test was used to compare control parameters with those obtained in $Co^{2+}$. n.s., non-significant difference with $P > 0.25$.

are shown when exceeding the symbol size. The parameters were compared by paired or independent Student's *t* test. The present study is based on recordings from 113 adapting-firing neurones (AFNs), 232 tonic-firing neurones (including 187 from Melnick *et al.* 2004) and 68 nucleated patches obtained from AFNs. All experiments, except those in Fig. 2*G* (right), were carried out at room temperature 22–24°C.

Ten AFNs were filled with 0.5% biocytin during recording for later cell visualization. Following the recording session, the slices with biocytin-filled neurones were transferred into a fixative containing 4% paraformaldehyde, 0.3% picric acid in 0.1 M phosphate buffer (pH 7.4) for one night. The slices were then washed in 0.1 M phosphate buffer saline (PBS) and treated with 30% sucrose for one night. After re-sectioning at 50 $\mu$m, slices were serially collected in PBS. After repeated washing (10 min each) in PBS containing 0.3% Triton X-100 (PBST), slices were incubated in an Alexa Streptavidin 594 antibody solution (1 : 1000 PBST, Molecular Probes, The Netherlands) at 4°C for 48 h. Slices were mounted in glycerol/PBS (3 : 1). Serial confocal optical sections were obtained with 1 $\mu$m steps at maximum pixel intensity. Images of labelled cells show the summed *Z* projection.

Computer simulations were done using NEURON software (Hines, 1993; Hines & Carnevale, 1997) and a model of a TFN described previously (Melnick *et al.* 2004). This universal model was created for SG neurones with diverse dendritic organizations. The input resistance and membrane time constants of the model were close to those described here for AFNs. Only three parameters of the model were varied in the present study: the $Na^+$ conductance ($g_{Na}$) in the axon initial segment and the voltage dependencies of $Na^+$ channel activation and inactivation. The $g_{Na}$ was changed from a control value of 1800 mS cm$^{-2}$ (1.0) to 730 mS cm$^{-2}$ (0.41) and 521 mS cm$^{-2}$ (0.29). The voltage dependencies were modified by uniformly shifting all equations describing $Na^+$ channel activation and inactivation by +5 and +11 mV, respectively.

## Results

Adapting-firing neurones (AFNs) were mostly found in the lateral part of SG (Fig. 2*A*). In ACSF they showed a resting potential of $-69.9 \pm 0.6$ mV ($n = 102$), an input resistance of $1.3 \pm 0.1$ GΩ ($n = 102$) and a membrane time constant of $84.5 \pm 5.0$ ms ($n = 20$). Unless otherwise stated, in the following current-clamp experiments the membrane potential was adjusted to −70 mV. AFNs were usually able to support firing only during the first 100–250 ms of depolarization evoked by an injection of 0.5 s pulses of inward current (Fig. 2*B*). The number of generated spikes depended on the pulse strength. In a narrow range of 10–40 pA it increased to a maximum of 3–6 spikes, but then became lower at stronger stimulation.

### $Ca^{2+}$-dependent conductances

A contribution of $Ca^{2+}$-dependent conductances to firing in AFNs was studied by using the inorganic blockers of $Ca^{2+}$ channels $Co^{2+}$, $Cd^{2+}$ and $Mg^{2+}$. The concentration of internal EGTA in these experiments was reduced to 1 mM. In the presence of 2 mM $Co^{2+}$ ($n = 10$), 0.1 mM $Cd^{2+}$ ($n = 8$) or 5 mM $Mg^{2+}$ ($n = 9$), no changes in firing pattern or the instantaneous frequency–current (*f–I*) characteristic, calculated for the first interspike interval, were observed (Fig. 2*C* and *D*, shown for $Co^{2+}$). The shape of single spikes was also unchanged by the blockers (Fig. 2*E*, shown for $Co^{2+}$). For 10 neurones recorded in control and $Co^{2+}$-containing solutions, several parameters of the single spike were compared and no significant difference was found (Table 1). The amplitude of after-hyperpolarization (fast and slow) was also not

reduced by $Co^{2+}$ ($n = 10$). Thus, it could be concluded that $Ca^{2+}$-dependent conductances do not contribute to discharge pattern in AFNs. In the following experiments we used the 10 mM EGTA pipette solution and both ACSF and ACSF* (0.1 mM $Ca^{2+}$ and 5 mM $Mg^{2+}$) as bath solution.

The effect of membrane potential on the firing pattern was studied in experiments where it was changed from −70 to −80 or −60 mV. Varying the potential in this range did not change the adapting firing patterns in either ACSF or ACSF* (Fig. 2*F*, shown for ACSF*, $n = 34$).

In 11 AFNs we tested whether lower external $K^+$ and increase in temperature to 35–37°C can change the basic pattern of intrinsic firing. In all these neurones a typical pattern of adaptation was seen in external 2.5 mM $K^+$ at room temperature (Fig. 2*G*, left) as well as after increasing the temperature to 35–37°C (Fig. 2*G*, right).

### $Na^+$ channels

$Na^+$ channels were studied using the $Cs^+$-containing pipette solution. The identification of a firing pattern

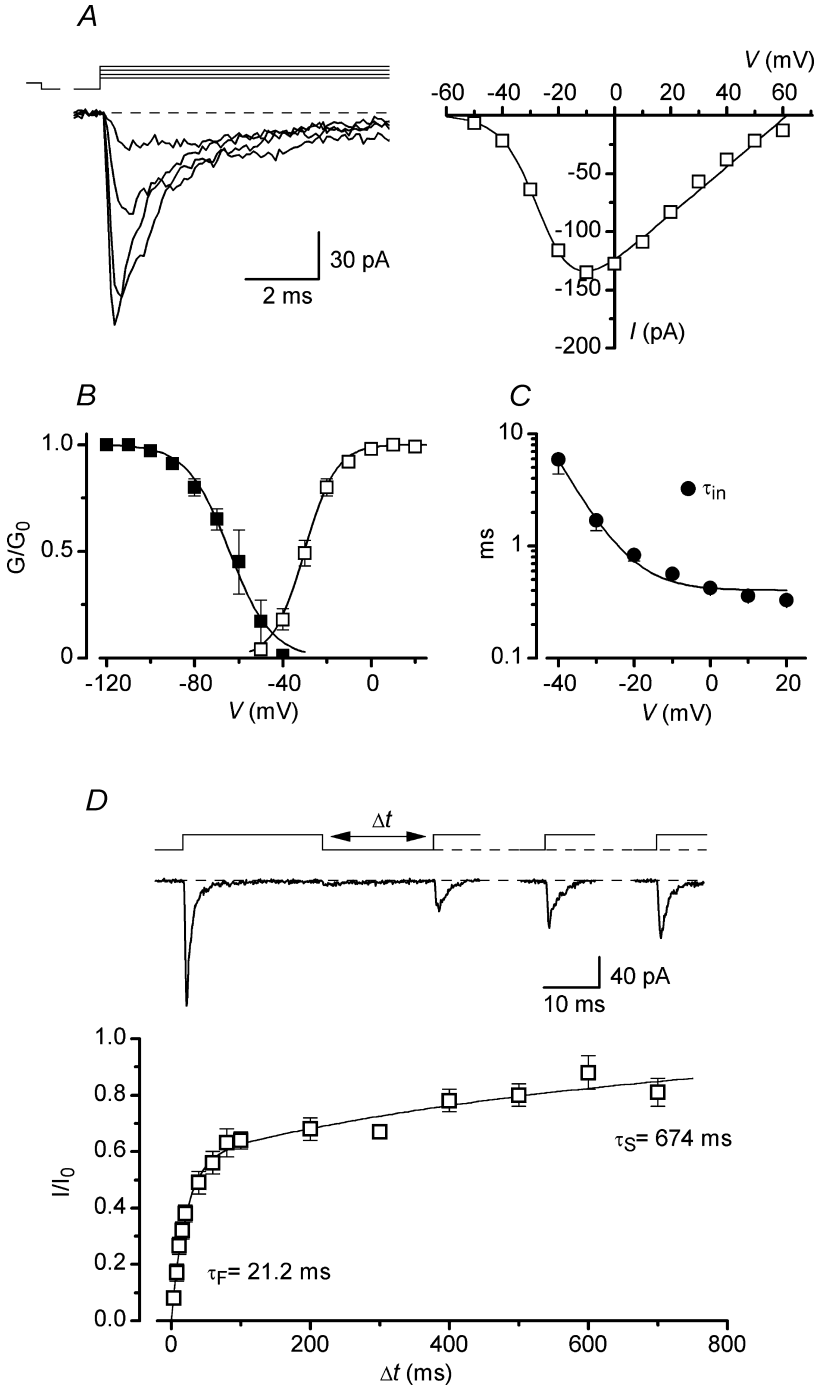


**Figure 3. Properties of $Na^+$ channels in nucleated patches from AFNs**
*A*, $Na^+$ currents activated by depolarization to −40, −30, −20 and −10 mV following a 50 ms prepulse to −120 mV. Holding potential, −80 mV. *I–V* curve is shown for the same neurone. *B*, steady-state activation and inactivation characteristics. Fitting parameters are given in the text. *C*, the inactivation time constant ($\tau_{in}$) as a function of membrane potential. *D*, kinetics of $Na^+$ channel recovery from inactivation. $Na^+$ currents activated by pairs of 25 ms pulses from −80 to −30 mV with varying intervals. The time course of $Na^+$ channel recovery from inactivation was fitted using a double-exponential function.

in a neurone was done during the first few seconds after membrane rupture, before $Cs^+$ replaced intracellular $K^+$ (Melnick *et al.* 2004). $Na^+$ currents were recorded in nucleated patches in ACSF* containing 1 mM TEA to reduce outward $K^+$ current (Fig. 3*A*). Their activation curve fitted with a Boltzmann equation had $V_{50} = -30.3 \pm 0.2$ mV and $k = 7.1 \pm 0.2$ mV (Fig. 3*B*, $n = 10$). The steady-state inactivation of $Na^+$ channels, studied with 50 ms conditioning prepulses, revealed a half-maximum inactivation at $-64.2 \pm 0.9$ mV and $k = -9.6 \pm 0.8$ mV (Fig. 3*B*, $n = 10$, test pulses to $-30$ or $-20$ mV). The inactivation kinetics of $Na^+$ channels could be fitted using a mono-exponential function with the time constant changing from $5.9 \pm 1.5$ ms at $-40$ mV to less than 0.5 ms at positive potentials (Fig. 3*C*, $n = 7$). Recovery of $Na^+$ channels from inactivation at $-80$ mV was studied by applying two 25 ms voltage pulses to $-30$ mV with varying intervals (Fig. 3*D*). The time course of recovery was double-exponential (Safronov & Vogel, 1995; Martina & Jonas, 1997; Melnick *et al.* 2004) with time constants of $21.2 \pm 2.2$ ms (57%) and $674 \pm 95$ ms (43%) ($n = 7$). The density of somatic $Na^+$ current in AFNs was $0.84 \pm 0.16$ pA $\mu m^{-2}$ ($n = 8$).

### Voltage-gated $K^+$ channels

The major $K^+$ current found in AFNs was a slowly inactivating delayed-rectifier ($K_{DR}$) current (Fig. 4*A*). For its recording the patch was held at $-80$ mV and depolarizing voltage pulses were applied after a 150 ms prepulse to $-60$ mV inactivating a fast transient $K^+$ ($K_A$) current. Half-maximum activation of $K_{DR}$ conductance was observed at $V_{50} = -18.0 \pm 0.6$ mV ($k = 9.3 \pm 0.5$ mV,M $n = 11$, Fig. 4*B*). The activation kinetics of the current was described by plotting the rise time of a half-maximum current ($\tau_{0.5}$) as a function of potential (Fig. 4*B*). The $\tau_{0.5}$ value became close to 1 ms at

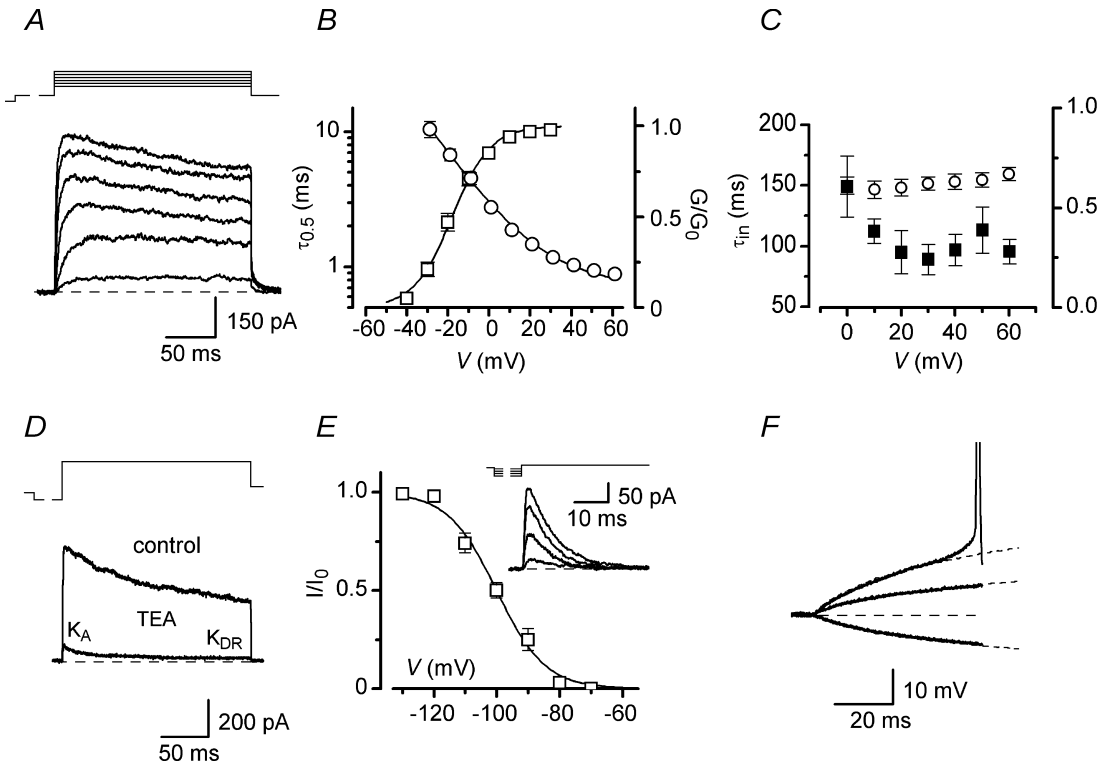


**Figure 4. Voltage-gated $K^+$ channels in AFNs**
*A*, $K_{DR}$ currents in patches activated in ACSF* by 200 ms depolarizing pulses (from $-30$ mV to $+20$ mV in a 10 mV step) following a 150 ms prepulse to $-60$ mV. Holding potential, $-80$ mV. These traces were off-line low-pass filtered at 1 kHz. *B*, steady-state activation curve (□) and the rise time of a half-maximum current ($\tau_{0.5}$, ○). *C*, the time constant of inactivation (■) and the ratio of currents measured at peak and at the end of the pulse (○) at different potentials. *D*, separation of transient $K_A$ currents in patches. Total $K^+$ current activated in a nucleated patch by a voltage step from $-120$ (150 ms) to $+60$ mV (200 ms) in the presence and absence of 10 mM TEA. Holding potential, $-80$ mV. *E*, steady-state inactivation of $K_A$ current. Whole-cell $K_A$ currents were recorded at $-50$ mV after a 150 ms prepulse to varying potentials ($-130$, $-110$, $-100$ and $-90$ mV). Holding potential, $-80$ mV. *F*, analysis of subthreshold current-clamp responses to injection of current pulses. AFN was stimulated by $-10$, $+10$ and $+20$ pA currents. A response to $-10$ pA current was considered as passive. It was digitally multiplied by factors of $-1$ and $-2$ (shown by dashed curves) and shown superimposed on the other two traces.

potentials positive to +30 mV (Fig. 4*B*, $n = 11$), indicating involvement of $K_{DR}$ current in spike repolarization. Starting from −20 mV a partial inactivation of $K_{DR}$ current developed. The time course and degree of inactivation were only weakly voltage dependent (Fig. 4*C*, $n = 11$). The reversal potential for $K_{DR}$ current, estimated from instantaneous tail currents, was close to $E_K$ of −84 mV ($n = 5$, not shown). In 10 mM TEA the current was blocked to 7.9 ± 1.0% ($n = 9$, not shown). The density of somatic $K_{DR}$ current in AFNs at +60 mV was 3.7 ± 0.3 pA $\mu m^{-2}$ ($n = 18$).

The $K_A$ component was not seen in nucleated patches when $K^+$ current was activated by a voltage step from −120 to +60 mV, but it could be separated after addition of 10 mM TEA as the fast inactivating component of the remaining current (Fig. 4*D*). The inactivation time constant of $K_A$ current was 10.5 ± 1.2 ms ($n = 10$). The amplitude of $K_A$ current, estimated from the double-exponential fitting of the inactivation kinetics of the remaining current, gave the somatic current density of 0.60 ± 0.17 pA $\mu m^{-2}$ at +60 mV ($n = 10$). Because of its low density in nucleated patches, the steady-state inactivation of $K_A$ current was studied in whole-cell mode. The whole-cell $K_A$ current evoked after a conditioning prepulse to −120 mV by a voltage step to potentials subthreshold for $Na^+$ channel activation (between −60 and −50 mV) ranged from 0 to 220 pA. The steady-state inactivation of $K_A$ current ($V_{50} = -96.3 \pm 1.2$ mV; $k = -7.2 \pm 0.8$ mV; $n = 5$) showed that it was completely inactivated at −70 mV (Fig. 4*E*). To reveal a possible contribution of $K_A$ current to setting the firing threshold in AFNs, the current-clamp responses of AFNs to depolarization were compared with membrane passive responses (Fig. 4*F*). A hyperpolarization evoked by a −10 pA current injection was considered as a passive response, which was appropriately scaled (dashed curves) and compared with cell responses to +10 and +20 pA depolarization (Fig. 4*F*). In agreement with our data about complete $K_A$ current inactivation at resting potential, a subthreshold depolarization was found to be passive and not affected by activation of $K_A$ conductance ($n = 28$).

By comparing the present results for AFNs with those recently reported for tonic-firing neurones (TFNs) from Melnick *et al.* (2004), it was possible to conclude that both neurone types possess $Na^+$ and $K_{DR}$ currents as well as negligible $K_A$ current. The ranges of $K_{DR}$ channel activation were very similar ($V_{50}$, −18.0 mV for AFNs *versus* −19.8 mV for TFNs). The kinetics of $Na^+$ channel recovery from inactivation in both cell types were two-exponential with the time constants: 21.2 ms (57%) and 674 ms (43%) for AFNs *versus* 21.8 ms (63%) and 793 ms (37%) for TFNs. The activation characteristics of $Na^+$ channels were insignificantly different ($V_{50}$, −30.3 mV for AFNs *versus* −35.7 mV for TFNs; $P < 0.1$). However, the density of somatic $Na^+$ and $K_{DR}$ currents in AFNs was lower and the $Na^+$ channel inactivation was shifted to more positive potentials by 11 mV ($V_{50}$, −64.2 mV for AFNs *versus* −75.5 mV for TFNs; $P < 0.02$). The following experiments were done to find out which of these factors played a critical role in the appearance of firing adaptation.

### Block of $Na^+$ rather than $K_{DR}$ channels in TFNs induces adaptation typical of AFNs

Since somatic $Na^+$ current represents only few per cent of the total $Na^+$ current in a spinal neurone (Safronov *et al.* 1997, 1999; Alessandri-Haber *et al.* 1999), a comparison of total $Na^+$ conductances in AFNs and TFNs was done by measuring maximum spike depolarization rates. The histogram of distributions of maximum de- and repolarization rates obtained by digital differentiation of the first spike in a train are shown in Fig. 5*A* for 102 AFNs and 232 TFNs. The mean maximum depolarization rates of 103.7 ± 2.8 V $s^{-1}$ for AFNs ($n = 102$) and 208.3 ± 3.4 V $s^{-1}$ for TFNs ($n = 232$) were significantly different ($P < 0.0001$). Since the depolarization rate is proportional to the inward current charging the membrane according to the equation: $I = C(dV/dt)$, where $C$ is membrane capacitance, our results imply relatively lower $Na^+$ conductance in AFNs in comparison with TFNs. In addition, the velocity of repolarization was also lower in AFNs (61.2 ± 1.5 V $s^{-1}$, $n = 102$, for AFNs *versus* 99.9 ± 1.9 V $s^{-1}$, $n = 232$, for TFNs, $P < 0.0001$).

In 10 TFNs, the effect of partial $K_{DR}$ current block on firing pattern was studied in ACSF*. In 5 of them an addition of 1 mM TEA resulted in the appearance of spike doublets in the train (Fig. 5*B*, left). In the other 5 TFNs, 1 mM TEA prolonged spikes, reduced the after-hyperpolarization and stability of firing, so that the amplitude of spikes progressively decreased during the train (Fig. 5*B*, right). However, both modified firing patterns were obviously different from those of AFNs.

In 21 TFNs the effect of TTX on pattern was studied in ACSF*. In all TFNs tested, the tonic firing changed to adapting and then to strongly adapting with a single spike when perfusion of the slice with 40 nM TTX-containing solution was started (Fig. 5*C*). Wash out of TTX was done just after the pattern modification occurred (before 40 nM TTX completely diffused into the slice). Differentiation of the voltage traces has shown that the appearance of adaptation correlated with a reduction of $Na^+$ current (Fig. 5*C*, bottom). In control solution, $Na^+$ current (estimated from derivatives) decreased during tonic firing due to the channel inactivation (Melnick *et al.* 2004) but still remained sufficiently large to support firing. After a partial $Na^+$ current block by TTX, only the first few spikes

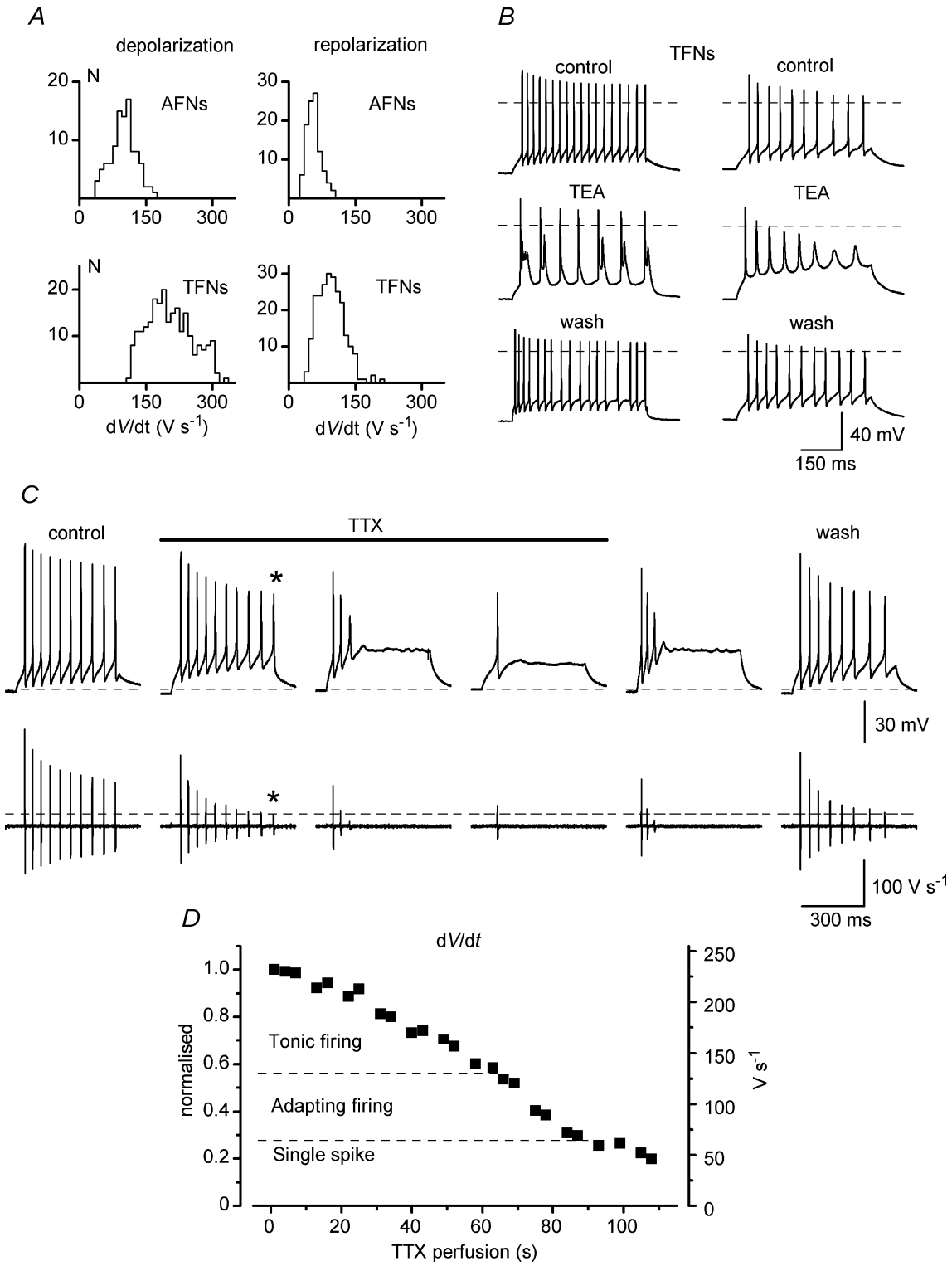


**Figure 5. TTX but not TEA can induce adaptation in tonic-firing neurones (TFNs)**
*A*, histograms of distribution of de- and repolarization rates in AFNs and TFNs. Bin width, 10 V $s^{-1}$. *B*, modifications of discharge patterns in TFNs by 1 mM TEA. *C*, induction of adaptation in a TFN during perfusion of the slice with 40 nM TTX. Bottom traces are derivatives of voltage traces (d*V*/d*t*). The baselines are 0 V $s^{-1}$. Dashed line shows the maximum depolarization rate for the reduced spike with the overshoot close to 0 mV (indicated by asterisks). *D*, modification of firing pattern from tonic to adapting as a function of $Na^+$ channel block during slice perfusion with 40 nM TTX. The maximum depolarization rate of the first spike in a train (right axis) is also shown as normalized to the control value (left axis).

could be generated before inactivation further reduced $Na^+$ current to the level below that necessary for the spike generation (dashed line). It should be noted that the block of $Na^+$ conductance also resulted in a reduction in the rate of spike repolarization, probably because of lesser activation of $K_{DR}$ channels by spikes with reduced overshoots. A transition from tonic to adapting firing occurred at 40–60% block of $Na^+$ conductance (Fig. 5*D*). Thus, block of $Na^+$ rather than $K_{DR}$ channels in TFNs modified a firing pattern to that typical of AFNs.

### Anatomy of AFNs

In order to test whether the smaller $Na^+$ conductance observed in AFNs might result from the cutting of the axon during the preparation of slices, AFNs were labelled by including biocytin in the patch pipette ($n = 10$). Because of their predominant location in the lateral part of SG (Fig. 2*A*), AFNs were rarely seen in sagittal sections typically used for anatomical studies. Therefore, the labelling was performed in transverse slices. All AFNs had small rounded somata and dense dendritic trees mostly staying within SG. Dendritic arbors exhibited spines and a limited spread in the medio-lateral or dorso-ventral dimensions. The axon was identified as a thinner process with constant diameter lacking spines. The axons branched extensively and entered laminae I and III. In some AFNs labelled axon branches had a total length of several hundreds of micrometres (Fig. 6*A* and *B*). Thus it could be concluded that the axon initial segment in AFNs was not cut during the preparation of slices.

### Computer simulation

Computer simulations were done to study how a reduction in $Na^+$ current and a shift in its activation and inactivation characteristics to more positive potentials can influence firing in a model neurone (Fig. 7). A control model of a TFN (Melnick *et al.* 2004) generated sustained firing with frequency increasing with stimulation intensity (Fig. 7, 1/0/0). The maximum depolarization rate of the first spike in a train was 231 V $s^{-1}$ when measured at +30 pA stimulation. By reducing the $Na^+$ conductance ($g_{Na}$) to 0.41 it was possible to induce firing adaptation (0.41/0/0). The maximum depolarization rate of the first spike in a burst was reduced to 132 V $s^{-1}$ (+30 pA stimulation). If the activation characteristics of $Na^+$ channels were shifted by +5 mV, a strong adaptation appeared in the model already at the control $g_{Na}$ value (1/+5/0). After the inactivation was shifted by +11 mV, the model again generated tonic firing (1/+5/+11). In the model with both activation and inactivation shifted to positive potentials a stronger reduction in $g_{Na}$ to 0.29 was needed for the induction of adaptation in the whole stimulation range (0.29/+5/+11). In this case the maximum depolarization rate of the first spike became 147 V $s^{-1}$ (+ 30 pA stimulation). Thus, both a reduction in $g_{Na}$ and a positive shift in activation characteristics promote spike frequency

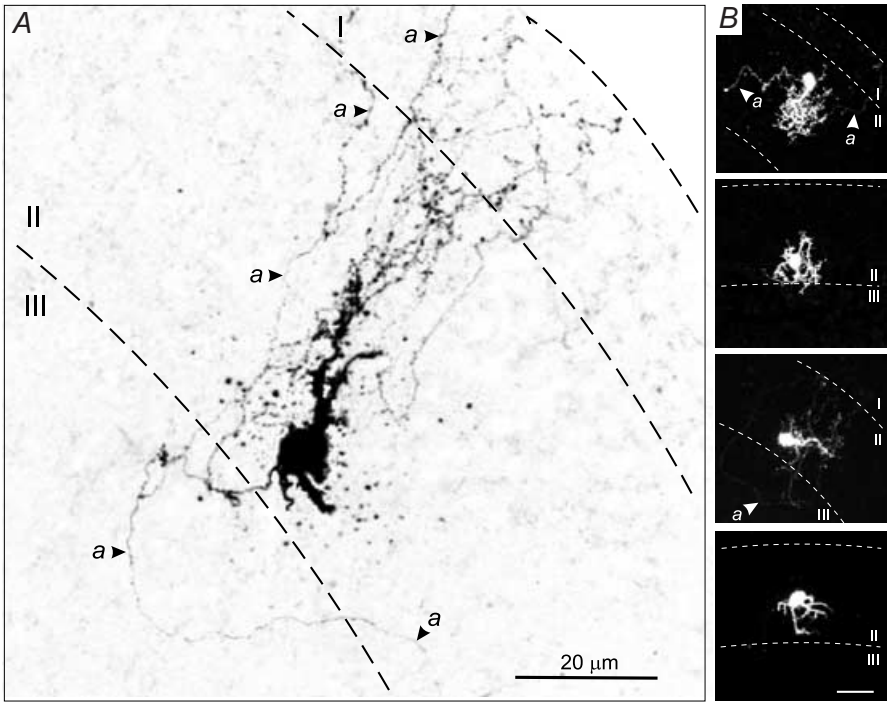


**Figure 6. Confocal images of AFNs labelled with biocytin**
*A*, inverted image of AFN with extensive axonal collaterals indicated by arrows. *B*, images of another four AFNs two of which have extensive axonal collaterals. Calibration bar, 20 $\mu$m. Dashed lines represent the borders between laminae I, II (SG) and III.

adaptation, while a positive shift in inactivation has an opposite effect.

## Discussion

This study has shown that reduced expression of $Na^+$ channels is a critical factor determining the appearance of spike frequency adaptation in SG neurones. Therefore, regulation of the intrinsic firing pattern in a SG neurone through modulation of $Na^+$ channels may represent an important element of spinal sensory encoding.

The degree of spike frequency adaptation is a criterion most frequently used for electrophysiological classification of superficial dorsal horn neurones (Thomson *et al.* 1989; Lopez-Garcia & King, 1994; Grudt & Perl, 2002;

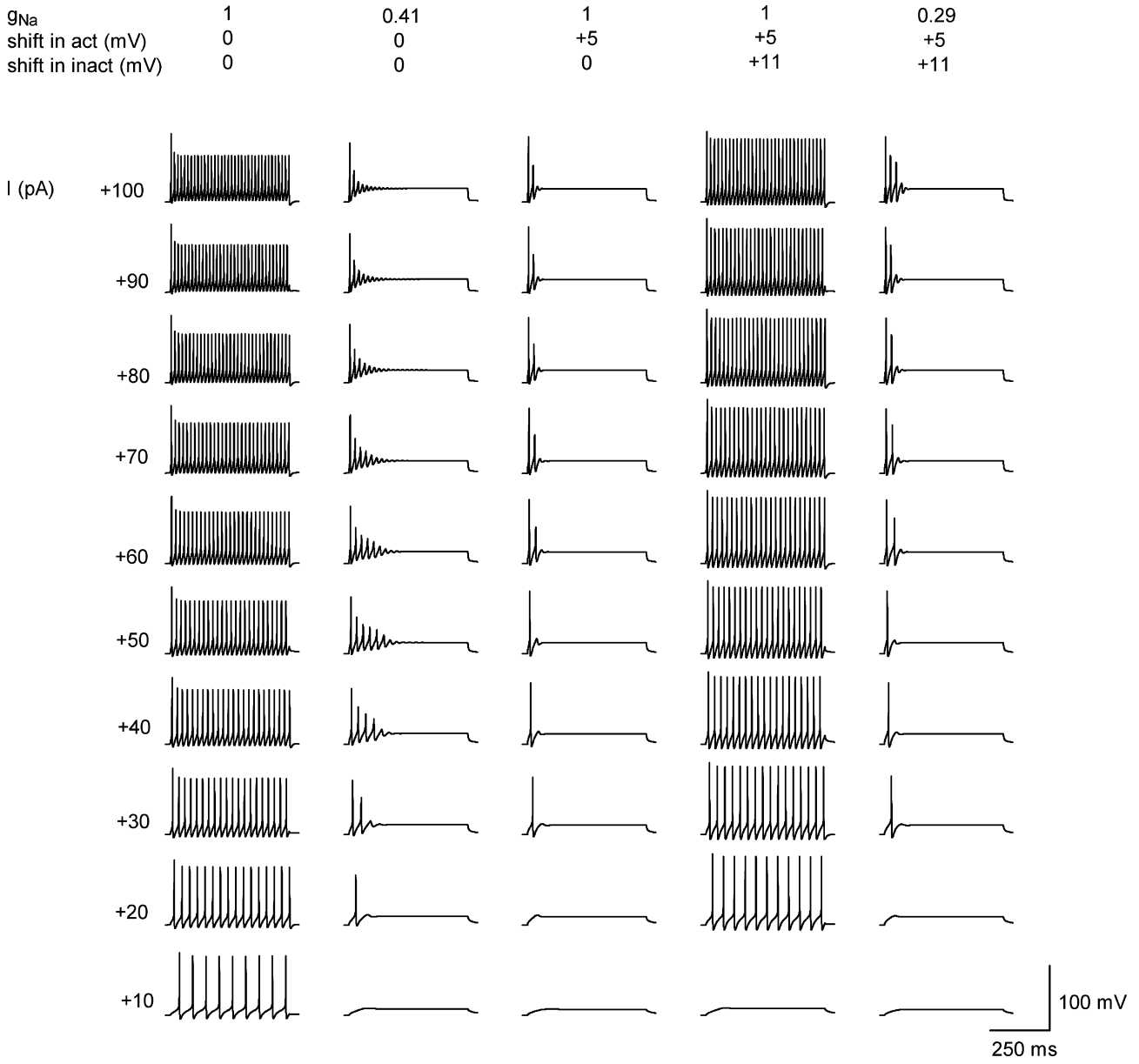


**Figure 7. Computer simulation of firing adaptation in SG neurone**
A basic model of TFN from Melnick *et al.* (2004). Repetitive firing evoked by 500 ms current pulses of increasing intensity in a basic model (1/0/0). Reduction of $Na^+$ conductance ($g_{Na}$) in the axon initial segment to 0.41 induced firing adaptation (0.41/0/0). An activation shift by +5 mV, without lowering $g_{Na}$, resulted in a strong firing adaptation (1/+5/0). A +11 mV shift in inactivation characteristics restored tonic firing in a model with control $g_{Na}$ (1/+5/+11). Reduction in $g_{Na}$ to 0.29 induced spike frequency adaptation in a model with shifted activation and inactivation characteristics (0.29/+5/+11). The resting potential was −70 mV in all simulations.

Prescott & De Koninck, 2002; Ruscheweyh & Sandkuhler, 2002; Hu & Gereau, 2003). Adapting-firing neurones (AFNs) which generate a short burst of spikes at the beginning of depolarization were also called phasic-, burst- or transient-type neurones. Most were physiologically classified as nociceptive-specific neurones (Lopez-Garcia & King, 1994). AFNs from lamina II (SG) receive monosynaptic input from slowly conducting primary C-type afferents (Grudt & Perl, 2002). Our data support a number of reports showing that adapting firing patterns are generated by only a subpopulation of neurones (Thomson *et al.* 1989; Lopez-Garcia & King, 1994; Grudt & Perl, 2002; Hu & Gereau, 2003; Melnick *et al.* 2004) rather than by all neurones in SG (lamina II) as proposed by Ruscheweyh & Sandkuhler (2002).

The present study shows that $Ca^{2+}$-dependent conductances do not contribute to the discharge pattern in AFNs. In this respect AFNs differ from tonic-firing neurones (TFNs), where $Ca^{2+}$-dependent slow after-hyperpolarization (AHP) regulated discharge rate and stabilized the basic form of tonic firing generated by voltage-gated $Na^+$ and delayed-rectifier $K_{DR}$ currents (Melnick *et al.* 2004). The present finding can also explain a difference in the shape of the AHP seen between TFNs (prolonged and polyphasic) and AFNs (short and monophasic) (Thomson *et al.* 1989; Prescott & De Koninck, 2002).

Voltage-gated $K^+$ channels are similar in both AFNs and TFNs. Fast inactivating $K_A$ current was found to be very small and strongly inactivated at resting potential and it was also not activated by a subthreshold depolarization. The lack of $K_A$ current appears to be important for the generation of typical discharge patterns in AFNs as well as TFNs, since the expression of large $K_A$ currents was shown to result in delayed-onset firing or irregular bust-like discharges (Yoshimura & Jessell, 1989; Grudt & Perl, 2002; Ruscheweyh & Sandkuhler, 2002). $K_{DR}$ current formed a major $K^+$ conductance in both AFNs and TFNs and had similar kinetics and activation ranges. Although $K_{DR}$ channels are necessary for the maintenance of sustained firing in TFNs (Melnick *et al.* 2004), their partial block by TEA did not result in the appearance of the typical pattern of spike frequency adaptation seen in AFNs. Thus, $K_A$ and $K_{DR}$ currents are unlikely to be responsible for the firing adaptation in SG neurones studied here.

Although the basic properties of $Na^+$ channels in AFNs were similar to those in TFNs (Melnick *et al.* 2004), their expression was lower and voltage dependency was slightly shifted to more positive potentials. Experiments with TTX and computer simulations have shown that a reduction in $Na^+$ conductance is critical for the appearance of adaptation. Simulations have also revealed a dual effect of a positive shift in voltage dependency of $Na^+$ channels on firing behaviour. Although the activation shift promoted spike frequency adaptation, a stronger shift in inactivation characteristics had an opposite effect. Thus, a lower $Na^+$ conductance seems to be a major factor introducing adaptation in SG neurones.

It is possible that $Na^+$ channels in AFNs and TFNs are formed by different combinations of principal ($\alpha$) and auxiliary ($\beta1$ and $\beta2$) subunits (Black *et al.* 1994; Waxman *et al.* 1999; Blackburn-Munro & Fleetwood-Walker, 1999). In this case, the change in subunit expression as well as the up-regulation of $Na^+$ channels associated with neuropathic pain (Waxman *et al.* 1999; Blackburn-Munro *et al.* 1999; Hains *et al.* 2003) can lead to hyperexcitability of dorsal horn neurones via the induction of long-term plasticity of their intrinsic firing properties. Besides, a regulation of $Na^+$ channels through an integration of cell-specific G-protein-coupled synaptic inputs (Ma *et al.* 1994; Carr *et al.* 2003) may introduce a short-term modulation of intrinsic firing and thus dynamic modification of spinal sensory encoding.

The smaller $Na^+$ conductance in AFNs is unlikely to result from axonal injury during the slicing procedure, as all AFNs labelled with biocytin possessed extensively branching axons crossing the borders with neighbouring laminae I and III. Labelled parts of axons were considerably longer than the 25 $\mu$m needed for spike generation in SG neurones (Safronov, 1999; Safronov *et al.* 1999). AFNs studied here belonged to one morphological class with its predominant localization in the lateral part of SG. The dendritic tree of AFNs has probably a rostro-caudal orientation within SG. Morphologically, AFNs were similar to islet cells (Gobel, 1978; Gobel *et al.* 1980; Todd, 1988; Eckert *et al.* 2003), although a strict conclusion could not be drawn based on neuronal images in transverse sections.

In conclusion, we suggest that different expression of $Na^+$ channels may be responsible for variation in the degree of spike frequency adaptation in SG neurones. The present results also imply that a modulation of $Na^+$ channels can represent an effective mechanism altering the firing behaviour of SG neurones. In addition to metabolic regulation of inwardly rectifying and A-type $K^+$ channels (Derjean *et al.* 2003; Hu & Gereau, 2003), a cell-specific modulation of $Na^+$ conductance provides one more mechanism of sensory, i.e. nociceptive, encoding and processing in the spinal cord.

## References

Alessandri-Haber N, Paillart C, Arsac C, Gola M, Couraud F & Crest M (1999). Specific distribution of sodium channels in axons of rat embryo spinal motoneurones. *J Physiol* **518**, 203–214.

Bentley GN & Gent JP (1994). Electrophysiological properties of substantia gelatinosa neurones in a novel adult spinal slice preparation. *J Neurosci Meth* **53**, 157–162.

Black JA, Yokoyama S, Higashida H, Ransom BR & Waxman SG (1994). Sodium channel mRNAs I, II and III in the CNS: cell-specific expression. *Brain Res Mol Brain Res* **22**, 275–289.

Blackburn-Munro G & Fleetwood-Walker SM (1999). The sodium channel auxiliary subunits beta 1 and beta 2 are differentially expressed in the spinal cord of neuropathic rats. *Neuroscience* **90**, 153–164.

Brown AG (1981). *Organization in the Spinal Cord*. Springer-Verlag, Berlin, Heidelberg.

Carr DB, Day M, Cantrell AR, Held J, Scheuer T, Catterall WA & Surmeier DJ (2003). Transmitter modulation of slow, activity-dependent alterations in sodium channel availability endows neurons with a novel form of cellular plasticity. *Neuron* **39**, 793–806.

Cervero F (1987). Dorsal horn neurones and their sensory inputs. In *Spinal Afferent Processing*, ed. Yaksh TL, pp. 197–216. Plenum Press, New York.

Chery N, Yu XH & De Konink Y (2000). Visualization of lamina I of the dorsal horn in live adult rat spinal cord slices. *J Neurosci Meth* **96**, 133–142.

Derjean D, Bertrand S, LeMasson G, Landry M, Morisset V & Nagy F (2003). Dynamic balance of metabotropic inputs causes dorsal horn neurons to switch functional states. *Nature Neurosci* **6**, 274–281.

Eckert WA, McNaughton KK & Light AR (2003). Morphology and axonal arborization of rat spinal inner lamina II neurons hyperpolarized by $\mu$-opioid-selective agonists. *J Comp Neurol* **458**, 240–256.

Edwards FA, Konnerth A, Sakmann B & Takahashi T (1989). A thin slice preparation for patch clamp recordings from neurones of the mammalian central nervous system. *Pflugers Arch* **414**, 600–612.

Gobel S (1978). Golgi studies of the neurons in layer II of the dorsal horn of the medulla (trigeminal nucleus caudalis). *J Comp Neurol* **180**, 395–414.

Gobel S, Falls WM, Bennet GJ, Abdelmoumene M, Hayashi H & Humphrey E (1980). An EM analysis of the synaptic connections of horseradish peroxidase-filled stalked cells and islet cells in the substantia gelatinosa of adult cat spinal cord. *J Comp Neurol* **194**, 781–807.

Grudt TJ & Perl ER (2002). Correlations between neuronal morphology and electrophysiological features in the rodent superficial dorsal horn. *J Physiol* **540**, 189–207.

Hains BC, Klein JP, Saab CY, Craner MJ, Black JA & Waxman SG (2003). Upregulation of sodium channel Nav1.3 and functional involvment in neuronal hyperexcitability associated with central neuropathic pain after spinal cord injury. *J Neurosci* **23**, 8881–8892.

Hines ML (1993). NEURON – a program for simulation of nerve equation. In *Neural Systems: Analysis and Modeling*, ed. Eeckman FH, pp. 127–136. Kluwer Academic Publishers, Boston.

Hines ML & Carnevale NT (1997). The NEURON simulation environment. *Neural Comput* **9**, 1179–1209.

Hu H-J & Gereau RW (2003). ERK integrates PKA and PKC signaling in superficial dorsal horn neurons. II. Modulation of neuronal excitability. *J Neurophysiol* **90**, 1680–1688.

LaMotte C (1977). Distribution of the tract of Lissauer and the dorsal root fibers in the primate spinal cord. *J Comp Neurol* **172**, 529–561.

Light AR & Perl ER (1977). Differential termination of large-diameter and small-diameter primary afferent fibers in the spinal dorsal gray matter as indicated by labelling with horse-radish peroxidase. *Neurosci Lett* **6**, 59–63.

Lopez-Garcia JA & King AE (1994). Membrane properties of physiologically classified rat dorsal horn neurons *in vitro*: correlation with cutaneous sensory afferent input. *Eur J Neurosci* **6**, 998–1007.

Ma JY, Li M, Catterall WA & Scheuer T (1994). Modulation of brain $Na^+$ channels by a G-protein-coupled pathway. *Proc Natl Acad Sci U S A* **91**, 12351–12355.

Magistretti J, Mantegazza M, de Curtis M & Wanke E (1998). Modalities of distortion of physiological voltage signals by patch-clamp amplifiers: a modeling study. *Biophys J* **74**, 831–842.

Magistretti J, Mantegazza M, Guatteo E & Wanke E (1996). Action potentials recorded with patch-clamp amplifiers: are they genuine? *Trends Neurosci* **19**, 530–534.

Martina M & Jonas P (1997). Functional differences in $Na^+$ channel gating between fast-spiking interneurones and principal neurones of rat hippocampus. *J Physiol* **505**, 593–603.

Melnick IV, Santos SFA, Szokol K, Szucs P & Safronov BV (2004). Ionic basics of tonic firing in spinal substantia gelatinosa neurons of rat. *J Neurophysiol* **91**, 646–655.

Prescott SA & De Koninck Y (2002). Four cell types with distinctive membrane properties and morphologies in lamina I of the spinal dorsal horn of the adult rat. *J Physiol* **539**, 817–836.

Rethelyi M (1977). Preterminal and terminal axon arborizations in the substantia gelatinosa of cat's spinal cord. *J Comp Neurol* **172**, 511–521.

Ruscheweyh R & Sandkuhler J (2002). Lamina-specific membrane and discharge properties of rat spinal dorsal horn neurones *in vitro*. *J Physiol* **541**, 231–244.

Safronov BV (1999). Spatial distribution of $Na^+$ and $K^+$ channels in spinal dorsal horn neurones: role of the soma, axon and dendrites in spike generation. *Prog Neurobiol* **59**, 217–241.

Safronov BV & Vogel W (1995). Single voltage-activated $Na^+$ and $K^+$ channels in the somata of rat motoneurones. *J Physiol* **487**, 91–106.

Safronov BV, Wolff M & Vogel W (1997). Functional distribution of three types of $Na^+$ channel on soma and processes of dorsal horn neurones of rat spinal cord. *J Physiol* **503**, 371–385.

Safronov BV, Wolff M & Vogel W (1999). Axonal expression of sodium channels in rat spinal neurones during postnatal development. *J Physiol* **514**, 729–734.

Sather W, Dieudonné S, MacDonald JF & Ascher P (1992). Activation and desensitization of *N*-methyl-D-aspartate receptors in nucleated outside-out patches from mouse neurones. *J Physiol* **450**, 643–672.

Sugiura Y, Lee CL & Perl ER (1986). Central projections of identified, unmyelinated (C) afferent fibers innervating mammalian skin. *Science* **234**, 358–361.

Thomson AM, West DC & Headley PM (1989). Membrane characteristics and synaptic responsiveness of superficial dorsal horn neurons in a slice preparation of adult rat spinal cord. *Eur J Neurosci* **1**, 479–488.

Todd AJ (1988). Electron microscope study of Golgi-stained cells in lamina II of the rat spinal dorsal horn. *J Comp Neurol* **275**, 145–157.

Waxman SG, Dib-Hajj S, Cummins TR & Black JA (1999). Sodium channels and pain. *Proc Natl Acad Sci U S A* **96**, 7635–7639.

Willis WD & Coggeshall RE (1991). *Sensory Mechanisms of the Spinal Cord*. Plenum Press, New York.

Yoshimura M & Jessell TM (1989). Membrane properties of rat substantia gelatinosa neurons in vitro. *J Neurophysiol* **62**, 109–118.

## Acknowledgements

We would like to thank Ms Helena Pereira for technical assistance. The work was supported by a grant from the Portuguese Foundation for Science and Technology (FCT).